IEEE Access
Multidisciplinary ⋮ Rapid Review ⋮ Open Access Journal

Received January 4, 2022, accepted January 15, 2022, date of publication January 18, 2022, date of current version January 27, 2022.

Digital Object Identifier 10.1109/ACCESS.2022.3144604

Triple-Element Back-to-Back Transducer With 3D Printed Housing for Intravascular Ultrasound Imaging: A Feasibility Study

HEE SU LEE, (Student Member, IEEE), AND JONG SEOB JEONG, (Member, IEEE)
Department of Biomedical Engineering, Dongguk University, Seoul 04620, South Korea

Corresponding author: Jong Seob Jeong (jjsspace@dongguk.edu)

This work was supported by the National Research Foundation (NRF) funded by the Korea Government under Grant 2021R1A2C1004329.

ABSTRACT Intravascular ultrasound (IVUS) can provide a high-resolution cross-sectional image of the blood vessel to detect the plaque morphology. The resolution of the IVUS image is proportional to a center frequency, however, a penetration depth decreases accordingly. To compensate for this problem, in this study, we propose the triple-element IVUS transducer capable of selecting an operating frequency according to the desired imaging area. In the proposed transducer, three-piezoelectric layers of 10 MHz, 20 MHz, and 30 MHz are formed on the top and both sides of the cube-shaped acoustic stack. These active layers share a common backing layer connected to one co-axial cable and can be driven simultaneously. In order to facilitate the manufacture process of the proposed IVUS transducer, split-assembling fabrication technique and a 3D printed housing with patterned electrodes were employed. The design specifications of the transducer were determined based on finite element analysis (FEA) simulation, and the prototype transducer was fabricated for feasibility study. The successful operation of individual elements constituting the proposed transducer was verified through B-mode imaging experiments using wire and tissue-mimicking phantoms. Subsequently, as a result of performing frequency compounding by combining two and three fundamental images, it was confirmed that the CNR (Contrast-to-Noise) value was improved by about 44%-77%. Therefore, the proposed IVUS transducer is expected to be one of the useful methods for diagnosing vascular diseases.

INDEX TERMS Intravascular ultrasound transducer, triple-element acoustic stack, back-to-back configuration, 3D printed housing, frequency compounding.

I. INTRODUCTION

Acute coronary syndrome (ACS) is a cardiovascular disease that causes heart attacks [1]–[4]. Atherosclerotic plaque, the main underlying disease of ACS, can cause thrombosis in the blood vessels by exposing internal substances to the outside due to rupture in a vulnerable state of plaque [5]–[7]. Most of plaque ruptures are caused in inflamed thin-cap fibroatheroma (TCFA) [2], [8], [9]. Since TCFA is defined as a thin fibrous cap, the intravascular imaging techniques with sufficient spatial resolution and penetration depth are required to accurately diagnose plaque vulnerability [10], [11]. Catheter-based intravascular ultrasound (IVUS) is a commonly used technique for more than 20 years allowing to image of cross-sectional view of coronary arteries. IVUS can be applied in a various fields such as measuring the size of vessel and lumen, detecting calcium severity, plaque imaging, and IVUS-guided stenting for stent deployment optimization [12], [13].

Typically, IVUS probes have a center frequency of 20 MHz to 40 MHz, an axial resolution of 70 μm to 200 μm, a lateral resolution of 200 μm to 400 μm, and a penetration depth of 5 mm to 10 mm [14]–[18]. In order to improve the spatial resolution using a single IVUS probe, several studies have been conducted on IVUS transducers with higher center frequencies. Lee *et al.* [19] improved the spatial resolution by an oblong-shaped focused transducer with 50 MHz center frequency, Yuan *et al.* [20] studied 60 MHz 1-3 composite transducer using PMN-PT, and Sung and Jeong [21] and Li *et al.* [22] fabricated 60 MHz and 80 MHz IVUS transducer using thin film-type PMN-PT, respectively. However, as the center frequency of the ultrasound transducer increases,

The associate editor coordinating the review of this manuscript and approving it for publication was Ravibabu Mulaveesala.

the depth of penetration decreases despite the improved resolution [23], [24]. In order to compensate the aforementioned limitation, several researches on the dual-element IVUS transducer capable of generating dual-frequency ultrasound have been conducted [23]–[29]. In this approach, a single probe can be used to drive low- and high-frequency components, respectively, to selectively improve spatial resolution and imaging depth. In addition, the frequency compound image capable of suppressing speckle pattern can be realized by combining obtained low- and high-frequency data [27]. The dual-layer transducer can also generate dual-frequency components. Here, the low-frequency layer was used to excite microbubbles, and the high-frequency layer was used for high-frequency ultrasound reception based on a non-linear response for super-harmonic imaging [30]–[32]. Although this method can provide high-contrast imaging, the size of the low-frequency layer should be longer than high-frequency layer resulting in reduced flexibility due to the increased front-rigid length. This issue is also generated in IVUS elastography using duel-element transducer in which low-frequency long-size element used for inducing shear wave and high-frequency short-size element used for elasticity imaging [33].

In general, by arranging two piezoelectric elements side-to-side, front-to-rear, and back-to-back, dual-frequency ultrasound can be generated. First, the side-to-side configuration arranges two elements in the lateral direction of the transducer with a slight interval between the elements [24]. This increases the outer diameter of the transducer, making it unsuitable for IVUS transducers used in blood vessels. In the case of front-to-rear configuration, since two elements are positioned in the elevational direction, the outer diameter does not change [25]–[27]. Nevertheless, since two images cannot be obtained simultaneously from the same cross section, each element should be run individually through a pull-back system, and the process of co-registering these images is very difficult. Although a focused-type transducer can be designed to achieve the same focal point, the front-to-rear configuration still reduces flexibility due to the increased front-rigid length of catheter [26], [27]. In the case of back-to-back configuration, the backing layers of the two elements are coupled to each other so as to transmit and receive ultrasound beam in opposite directions. Thus, in this configuration, small outer diameter can be achieved, which is suitable compact form factor for IVUS transducer [24], [28]–[30]. Also, it does not significantly affect flexibility of catheter since it has short front-rigid length. Furthermore, the two elements obtain images from identical cross-section resulting in easy co-registration.

Ma *et al.* [24] fabricated three types of back-to-back structure transducers with different frequency combination (35/90 MHz, 35/120 MHz, 35/150 MHz) and Munding *et al.* [28] combined 30/80 MHz dual-frequency transducer with a polyethylene (LDPE) sheath. Using the same transducer, Munding *et al.* [29] also obtained an in-vivo coronary vessel image of animal model and verified that dual-frequency IVUS transducer can be a potential intravascular imaging technique. Recently, a triple-frequency endoscopic transducer with three different elements has been proposed, which complements the conventional dual-element transducer with a wide gap between low and high frequencies and expands the frequency selection options depending on the desired imaging area [31] .

In the same vein, in this study, a triple-element back-to-back IVUS (TEBB_IVUS) transducer with a unique structure was proposed considering easy fabrication, minimal form factor, and reduced system complexity. The proposed technique can provide cross-sectional intravascular images for vascular diseases requiring high resolution, such as TCFA, while providing deep penetration depth. In addition, the proposed transducer allows the operator to select the appropriate driving frequency depending on the morphology of the imaging area. As the types of fundamental images with different center frequencies increase, the quality of IVUS image can be improved through more efficient frequency compounding by using various combinations of these images. In the designed transducer, three-piezoelectric elements share a square-shaped backing layer based on back-to-back configuration, allowing transmitting and receiving ultrasound at the left, right, and front sides of the acoustic stack. Manufacturing processes such as signal and ground wiring were simplified by using a three-dimensional (3D) printed IVUS housing designed specifically for the proposed technique. Additionally, only one co-axial cable was used to drive entire elements resulting in simplified driving system. Brightness-mode (B-mode) images of wire and tissue-mimicking phantoms were successfully obtained by the proposed transducer. Moreover, frequency compound images were implemented to achieve the enhanced contrast-to-noise ratio (CNR) by suppressing speckle pattern. Section II summarized the principles and design specifications of the proposed technique, and Section III explained the experimental results. Discussion and conclusion on the proposed technique were described in Section IV and Section V, respectively.

II. METHODS

A. CONFIGURATION AND DESIGN OF TEBB_IVUS TRANSDUCER

The schematic diagram of the acoustic stack of the proposed TEBB_IVUS transducer is shown in Fig. 1. The shape of the acoustic stack is a cube, and three types of piezoelectric layers are attached to each side. The size of the typical IVUS transducer is less than 1 mm for imaging inside narrow blood vessels. However, in this study, the size of the IVUS acoustic stack was determined to be 1.8 mm $\times$ 1.8 mm. That is, due to technical limitations of currently available 3D printed housings such as minimum wall thickness and limited hole diameters, the size of the space where the acoustic stack is located had to be 1.8 mm $\times$ 1.8 mm. In this configuration, in order to efficiently connect the signal line from the patterned electrode of the housing to the piezoelectric layer, the

TABLE 1. Specifications of the designed transducers for FEA simulation.

	Material	Density (kg/m^3)	Longitudinal Velocity (m/s)	Acoustic Impedance (MRayl)	Longitudinal Attenuation Coefficient (dB/mm @10 MHz)	Desired Thickness (μm)	Dimension (mm^2)
Piezoelectric Layer	CTS 3203 HD (PZT-5H) (for 10 MHz)	7820	4192.46	32.79		190 (for 10 MHz)	1.8 x 1.8
	APC 840 (PZT4) (for 20 MHz & 30 MHz)	7700	4684.87	36.07		93 (for 20 MHz) 64 (for 30 MHz)	
Matching Layer	Insulcast 501 + 0.5~1 μm Silver Particles	3860	1900	7.33		44 (for 10 MHz) 23 (for 20 MHz) 14 (for 30 MHz)	
Backing Layer	EJ-2189	3655	2071	7.57	26.56	900	

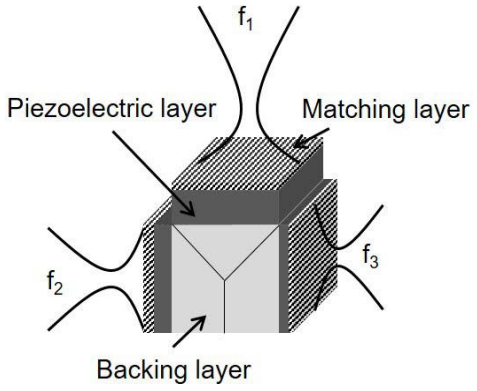

FIGURE 1. Schematic diagram of the acoustic stack of the proposed TEBB_IVUS transducer. f_1, f_2, and f_3 indicate different center frequencies.

aperture size should be maximally fit into this space. If the center frequency becomes higher while maintaining the aperture size to 1.8 mm × 1.8 mm, it leads to a greater electrical impedance mismatch with respect to 50 Ω. In addition to this size limitation, in consideration of the frequency range (20 MHz to 40 MHz) of the typical IVUS transducer, the center frequencies of each device were determined to be 10 MHz, 20 MHz, and 30 MHz, respectively. If advance in 3D printing technique can make IVUS housing smaller, we anticipate that the center frequency can be much higher because the smaller acoustic stack can be fabricated for intravascular imaging. Additionally, various piezoelectric materials were used to minimize the impedance mismatch with respect to 50 Ω according to the frequency and limited size of each element.

Finite element analysis (FEA) simulations using PZFlex (OnScale, Cupertino, CA, USA) were employed to determine the material and thickness of the piezoelectric and matching layers, taking into account the optimized sensitivity and electrical impedance of each element. In other words, to increase sensitivity of each element by overcoming the limited size of the acoustic stack, we used different piezoelectric material for each element. Specifically, PZT-5H (CTS3203HD, CTS Corp., Bolingbrook, IL, USA) for 10 MHz element and PZT4 (APC840, APC International, Ltd., Mackeyville, PA, USA) for 20 MHz and 30 MHz elements were chosen as piezoelectric materials. A mixture of 0.5 μm- 1 μm silver particles (Thermo Fisher Scientific Inc., Waltham, MA, USA) and unloaded epoxy (Insulcast 501, ITW Polymer Technologies, Montgomeryville, PA, USA) was used for a matching layer. A conductive epoxy EJ-2189 (Epoxy Technology Inc., Billerica, MA, USA) was used to make a backing layer. The specifications of the designed transducer are summarized in Table 1. Since FEA simulation was used for just extracting design parameters for fabrication, simulated results were not included in this paper.

B. 3D PRINTED HOUSING WITH ENGRAVED-PATTERN ELECTRODES

In general, most commercial single-element IVUS transducers use a wiring scheme suitable for mass production due to its low cost and relatively fast production speed [21]. In this method, a central wire of the micro-coaxial cable is attached to the matching layer with a conductive epoxy, while the shielding wire is connected to the backing layer for ground formation [25], [28], [29]. However, in this method, laying the wire on the matching layer and fixing it with adhesive are challenging works. Also, when rotating the catheter, proper adhesive force should be maintained so that the signal line and the matching layer are not separated by centrifugal force. Also, it is essential to minimize the distortion of transmitted and received ultrasound waves by minimizing the adhesive area.

In order to connect the electrodes of the proposed TEBB_IVUS transducer, more efficient solution is required because the wiring process should be performed three times. Therefore, in this study, the IVUS housing with engraved electrode patterns was proposed based on 3D printing technique to simplify the wiring connection process.

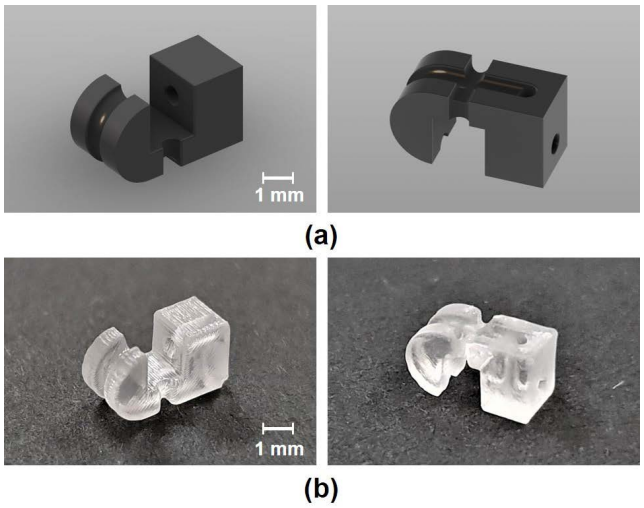

FIGURE 2. (a) 3D model of the proposed housing and (b) photograph of the 3D printed prototype housing.

The proposed housing was designed by computer-aided design (CAD) program Fusion 360 (Autodesk, Inc., San Rafael, CA, USA) as shown in Fig. 2 (a). The designed IVUS housing has thin grooves which exist along the surface of the housing and can be eventually connected to the surface of the matching layer. For the triple-element acoustic stack, the grooves are diverged into three sections to connect with each surface of three matching layers. This engraved grooves were filled with a conductive epoxy (CW2400, ITW Chemtronics, Kennesaw, GA, USA) to form electrode pattern, and the signal wire and acoustic stack are connected through this electrode pattern by attaching the central wire of the micro-coaxial cable at the beginning of the pattern.

In addition, there is a hole where the ground wire can pass through, and it allows the backing layer and ground wire to be connected. Consequently, it is expected that the proposed IVUS housing can simplify the manufacturing process and increase the convenience of electrode connection since the wire is not directly connected to the surface of matching layer. The proposed housing was produced by 3D printing technique (Creallo, Inc., Seoul, Korea) as shown in Fig. 2 (b).

C. FABRICATION OF DESIGNED TRANSDUCER

The prototype transducer was built to experimentally demonstrate the performance of the designed transducer. Fig. 3 describes the specific manufacture process of the proposed TEBB_IVUS transducer, called split-assembling fabrication, and photograph of the fabricated acoustic stack. First, one 10 mm × 10 mm × 0.5 mm PZT-5H and two 10 mm × 10 mm × 0.5 mm PZT4 plates were prepared. PZT-5H plate was lapped to get 190 μm thickness for 10 MHz, while PZT4 plates were lapped to obtain 93 μm and 64 μm for 20 MHz and 30 MHz, respectively. On the lapped surfaces, electrodes were formed by gold sputtering over the chrome seed layer. Subsequently, a mixture of 0.5 μm - 1 μm silver particles

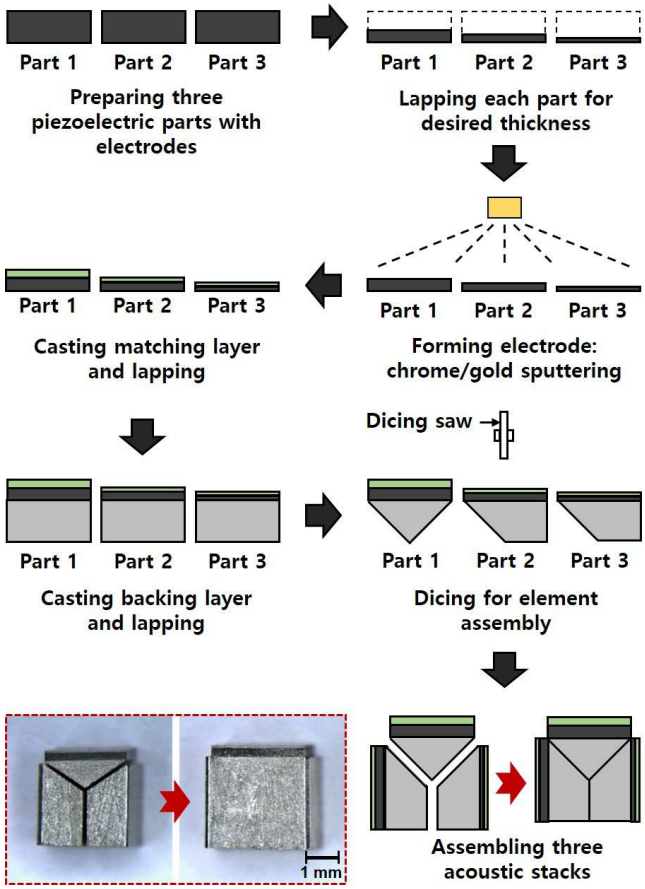

FIGURE 3. Schematic diagram for fabrication process of the proposed TEBB_IVUS transducer and photograph of assembled TEBB stack.

(Thermo Fisher Scientific Inc., Waltham, MA, USA) and unloaded epoxy (Insulcast 502, ITW Polymer Technologies, Montgomeryville, PA, USA) was casted on the surface of each piezoelectric layer and centrifuged to form the matching layer. The casted matching layers were lapped to get 44 μm, 23 μm, and 14 μm for 10 MHz, 20 MHz, and 30 MHz, respectively. After the stacks with piezoelectric layer and matching layer were turned over, a conductive epoxy EJ-2189 (Epoxy Technology Inc., Billerica, MA, USA) was casted on the face of each piezoelectric layer, forming the backing layers. For the element assembly, part 1 for 10 MHz was cut into triangular shape and part 2 and part 3 were cut into trapezoidal shapes with a dicing saw (DAD322, DISCO Corp., Tokyo, Japan). Finally, the diced elements were assembled by a conductive epoxy (CW2400, ITW Chemtronics, Kennesaw, GA, USA) to form a cube-type acoustic stack.

Fig. 4 shows the combining and bonding process for the assembled triple-element stack and 3D printed IVUS housing. Since the diameter of the IVUS catheter should be small for imaging inside narrow blood vessels, in the proposed technique, only a single coaxial cable was employed to drive three elements simultaneously. After separating the central wire and shielding wire of the single micro-coaxial cable, the central wire was placed on the starting point of the groove by

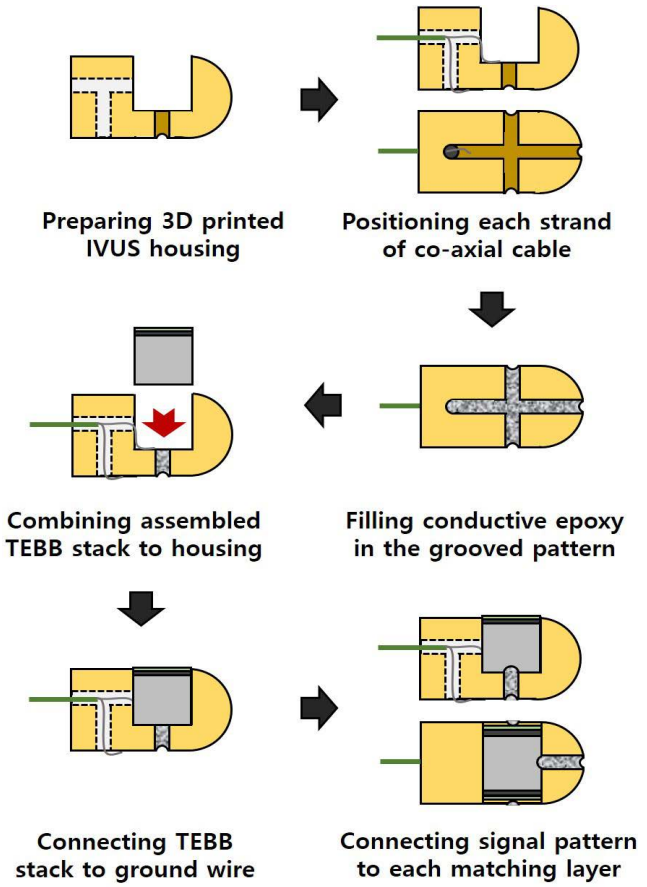

FIGURE 4. Schematic diagram of combined manufacturing process of TEBB stack and 3D printed housing.

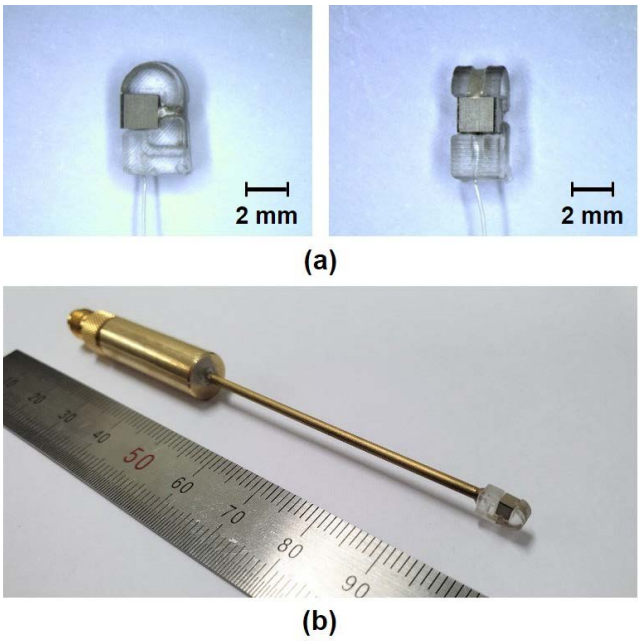

FIGURE 5. Photographs of (a) combined TEBB stack and 3D printed housing, and (b) overall view of fabricated TEBB_IVUS transducer.

passing through a hole at the bottom of the housing, while the shielding wire was positioned outwards through a central hole. After that, the engraved grooves were filled with a conductive epoxy to form electrode pattern, and the center wire was connected in the electrode pattern. The assembled element was carefully placed on the housing, allowing the backing layer to be in contact with the shielding wire and fixing them by a conductive epoxy. Thus, common ground was generated by connecting the shielding wire and all backing layers of assembled element. Subsequently, the electrode pattern was extended using additional conductive epoxy to slightly cover the edge of the matching layers so that the central wire can be connected to the surface of the acoustic stack using the electrode pattern as a bridge between them. In this way, all of three elements were connected in parallel by the electrode pattern, resulting in simplified system for driving multiple frequency components. The other side of the coaxial cable was connected to a sub-miniature version A (SMA) connector through a brass tube with 1.5 mm outer diameter. The fabricated TEBB stack and the prototype TEBB_IVUS transducer are shown in Fig. 5.

D. EXPERIMENTAL SETUP

To measure the performance of the fabricated transducer, electrical impedance was firstly measured by an impedance analyzer (4294A, Keysight, San Jose, CA, USA). Since each element in the proposed transducer is connected by one common coaxial cable, electrical impedance was measured before element assembly. Additionally, a pulse-echo test was conducted in the water container. A quartz was used as a reflector and placed about 10 mm away from the surface of the transducer. A 100 V_{pp} impulse signal with 2 ns pulse width was used as a driving signal for pulse-echo test. In the wire phantom B-mode imaging, a 100 V_{pp} impulse signal with a pulse width of 8 ns was used, and a reception gain was 30 dB. Since the intensity of the reflected signal from the wire target is strong enough, the impulse signal was used as a driving signal. Fig. 6(a) shows a block diagram of the experimental setup for B-mode imaging of tissue-mimicking phantoms. For the wire phantom experiment, in this setup, the function generator was replace with a pulser/receiver (UT340, UTEX Scientific Instrument Inc., Mississauga, ON, Canada), and a rotating motor was replaced with a linear motor.

Subsequently, B-mode images from the tissue-mimicking phantom were obtained. The input signals for three element were made by MATLAB (MathWorks Inc., Natick, MA, USA) software. The center frequency of each signal was determined in consideration of the pulse-echo test result, and the number of cycles of sine wave was selected to be 5 cycles according to the bandwidth of each element. The input signal was generated by a function generator (33600A, Keysight Technologies, Santa Clara, CA, USA) and amplified by an RF amplifier (75A250A, Amplifier Research, Souderton, PA, USA). The amplified signal was transmitted to the transducer through an expander and the reflected signal was transferred

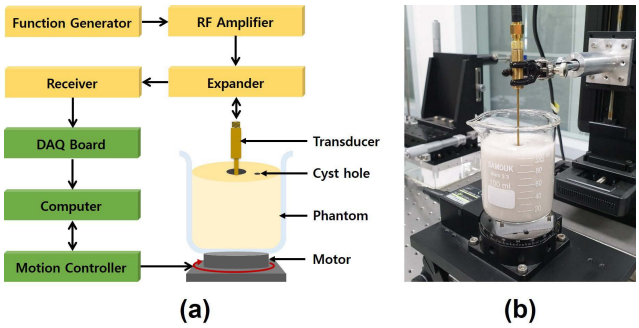

FIGURE 6. (a) Block diagram and (b) photograph of experimental setup for B-mode image acquisition using tissue-mimicking phantom.

to a receiver system with a 20 dB receive gain. A data acquisition (DAQ) board (CS121G2, GaGe Applied Technologies Inc., Lachine, QC, Canada), which was controlled by a LabVIEW (National Instruments., Austin, TX, USA) software program, gathered the received signals. During image acquisition, the tissue-mimicking phantom was 360° rotated by a motor and motion controller (SHOT-304GS, SIGMA KOKI, Tokyo, Japan) with 0.6° angle step. A customized wire phantom and a tissue-mimicking phantom were prepared for B-mode imaging test. The wire phantom was made of a tungsten wire with 25 μm diameter.

In the case of the tissue-mimicking phantom, aluminum oxide particles (Nanko Abrasive Industry Co., Ltd., Tokyo, and Japan) of 3 μm, 12 μm and 30 μm in size were prepared in 5:6:7 weight ratio for use as scatterers. Subsequently, they were mixed with gelatin powder (Geltech Co. Ltd., Busan, Korea) using water. The concentrations of scatterers and gelatin powder were 3% and 10%, respectively. A large hole with a diameter of 8 mm for inserting the transducer was made in the center of the phantom, and a small hole with a diameter of about 2 mm was made next to the central hole and filled with water. Note that the distance between a center of the large hole and a center of the small hole was 7 mm. Fig. 6(b) shows the fabricated tissue-mimicking gelatin phantom.

III. RESULTS

A. MEASURED PROPERTIES OF PROTOTYPE TEBB_IVUS TRANSDUCER

Fig. 7 shows the measured electrical impedance and pulse-echo data. The resonance frequencies of 10 MHz element were 8.66 MHz (54.06 Ω) and 13.34 MHz (43.4 Ω), and the anti-resonance frequencies were 9.83 MHz (159.7 Ω) and 14.69 MHz (116.6 Ω). The resonance frequencies of 20 MHz element were 16.9 MHz (25.97 Ω) and 26 MHz (19.19 Ω), and the anti-resonance frequencies were 19.18 MHz (50.21 Ω) and 28.98 MHz (32.98 Ω). Subsequently, the resonance frequencies of 30 MHz element were 25.35 MHz (10.37 Ω) and 38.27 MHz (9.04 Ω), and the anti-resonance frequencies were 28.1 MHz (23.39 Ω) and 42.13 MHz (12.5 Ω). In the case of the pulse-echo test, the 10 MHz element had 11.15 MHz center frequency, 50.67%

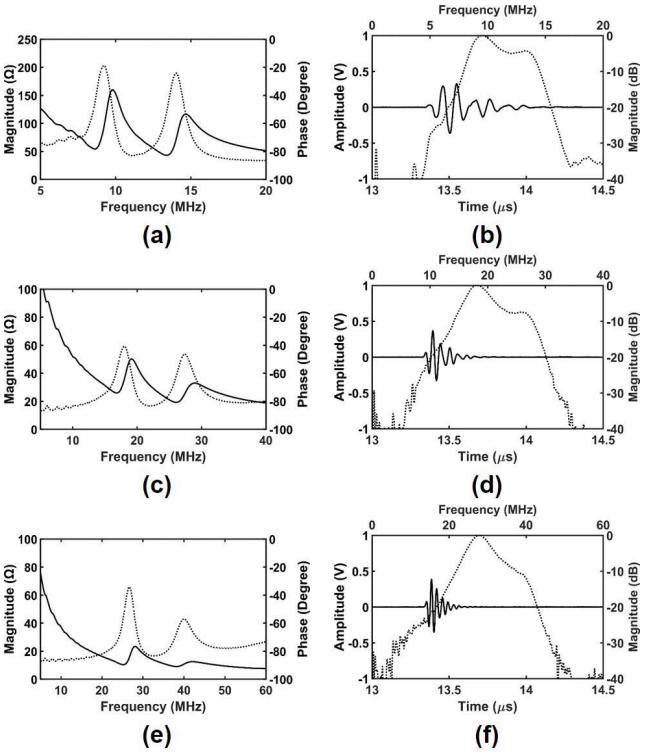

FIGURE 7. Property measurement results: electrical impedance of (a) 10 MHz element, (c) 20 MHz element, and (e) 30 MHz element (solid line: magnitude, dashed line: phase). Pulse-echo response of (b) 10 MHz element, (d) 20 MHz element, and (f) 30 MHz element (solid line: time domain response, dashed line: frequency domain response).

−6 dB fractional bandwidth, and 690.84 mV_{pp} sensitivity. The 20 MHz element had 18.77 MHz center frequency, 35.98% −6 dB fractional bandwidth, and 697.81 mV_{pp} sensitivity. The 30 MHz element had 28.22 MHz center frequency, 32.55% −6 dB fractional bandwidth, and 734.44 mV_{pp} sensitivity. Although the measured electrical impedance had wide range of difference between three elements, sensitivities were similar to each other. This phenomenon is mainly due to the different characteristics of PZT-5H and PZT4 used to fabricate each element. Additionally, experimental setup such as equipments and cables, and fabricating error including thickness errors of the piezoelectric and matching layers may affect the measured sensitivity of the prototype transducer.

B. B-MODE IMAGE OF WIRE PHANTOM

Fig. 8 shows the B-mode images of the wire phantom obtained by the TEBB_IVUS transducer. The acquired radio frequency (RF) data was filtered by a finite impulse response (FIR) band pass filter to remove noise and unwanted signals, resulting in extraction of the desired fundamental frequency component [34]. The envelope detection and log compression were conducted to realize B-mode mages. For the quantitative analysis of the spatial resolution of each image, the axial and lateral beam profiles were obtained from the B-mode images (Fig. 8) as shown in Fig. 9. The −6 dB axial beam widths of 10 MHz, 20 MHz, and 30 MHz

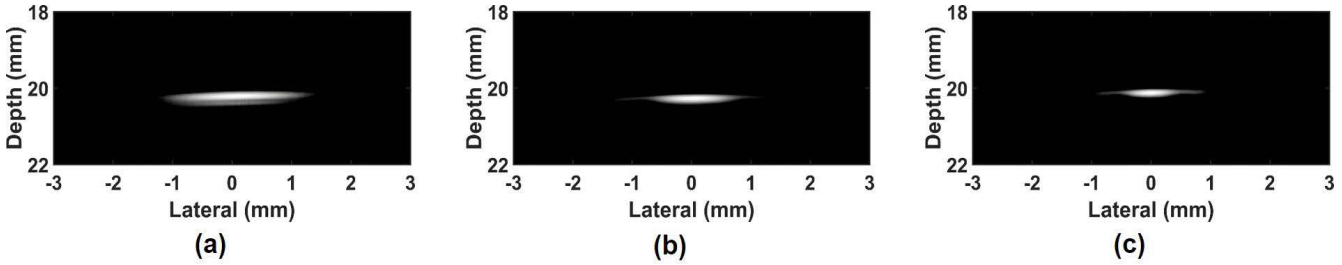

FIGURE 8. Wire phantom B-mode images: (a) 10 MHz, (b) 20 MHz, and (c) 30 MHz elements. The dynamic range of logarithmic compression was 20 dB for all images.

TABLE 2. Measured axial and lateral beam widths data of the wire phantom using the prototype TEBB_IVUS transducer.

	10 MHz	20 MHz	30 MHz
-6 dB Axial Beam Width (μm)	341	226	195
-6 dB Lateral Beam Width (μm)	2047	1297	930
-10 dB Axial Beam Width (μm)	494	303	257
-10 dB Lateral Beam Width (μm)	2666	2584	1947

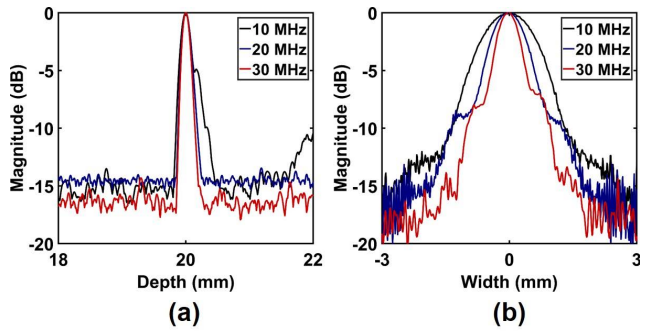

FIGURE 9. Beam profiles of wire phantom B-mode images in Fig. 8: (a) axial direction and (b) lateral direction.

images were 341 μm, 226 μm, and 195 μm, respectively, and -10 dB axial beam widths were 494 μm, 303 μm, and 257 μm, in the same order. The -6 dB lateral beam widths of 10 MHz, 20 MHz, and 30 MHz images were 2047 μm, 1297 μm, and 930 μm, respectively, and -10 dB lateral beam widths were 2666 μm, 2584 μm, and 257 μm, in the same order. These results were summarized in Table 2.

C. B-MODE IMAGE OF TISSUE-MIMICKING PHANTOM

Fig. 10 shows the B-mode images of the tissue-mimicking gelatin phantom using the TEBB_IVUS transducer. The dynamic range of logarithmic compression for all images was set to 30 dB. The white-dot marks visualized vertically indicate a 4 mm interval. The RF data was acquired based on the experimental setup described in Fig. 6, and post image implementation process was performed similar to wire phantom B-mode imaging. For image alignment, since the middle

TABLE 3. Calculated CNR values obtained from tissue-mimicking phantom images.

	Frequency Component	CNR
Fundamental Image	10 MHz	3.36
	20 MHz	3.61
	30 MHz	3.65
Frequency Compound Image	10 MHz + 20 MHz	5.10
	10 MHz + 30 MHz	5.11
	20 MHz + 30 MHz	5.12
	10 MHz + 20 MHz + 30 MHz	6.27

element of the triple-element acoustic stack was 10 MHz, 20 MHz fundamental image should be rotated by $-90°$ and 30 MHz fundamental image should be rotated by 90°. Thus, 150 scanlines were moved to align images because the raw data before generating the polar images had an angle step of 0.6° per scanline. Fig. 10(a)-(c) show the 10 MHz, 20 MHz, and 30 MHz fundamental images, respectively. Through the results of this experiment, it was confirmed that as the frequency increases, the resolution increases but the penetration depth decreases as well known.

Furthermore, frequency compounding was performed to suppress speckle noise and to increase the CNR for improved image quality and to demonstrate the feasibility of more efficient application of the proposed transducer. The RF data used for fundamental images was carried out Hilbert transform to obtain envelop detected signals. After that, the envelop signals were normalized due to the different maximum magnitude of each sub-band envelope signal. Subsequently, image alignment was processed and the polar images were generated. Finally, the frequency compound images were obtained by averaging out two fundamental images of 10 MHz and 20 MHz (Fig. 10(d)), 10 MHz and 30 MHz (Fig. 10(e)), and 20 MHz and 30 MHz (Fig. 10(f)), and combining three fundamental images of 10 MHz, 20 MHz, and 30 MHz (Fig. 10(g)). As a region of interest (ROI), two white boxes were selected and visualized in the images. One

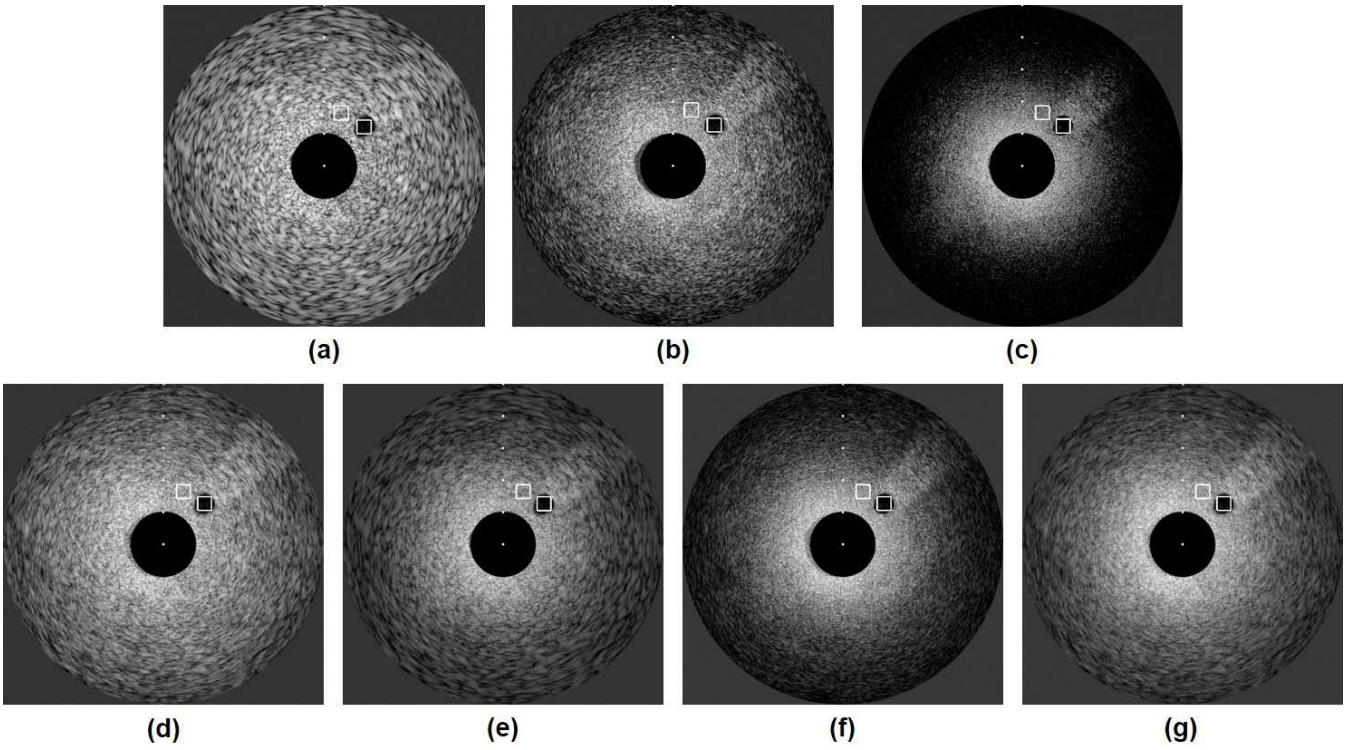

FIGURE 10. B-mode images of tissue-mimicking phantom: fundamental images of (a) 10 MHz, (b) 20 MHz, and (c) 30 MHz, and frequency compound images composed of (d) 10 MHz + 20 MHz, (e) 10 MHz + 30 MHz, (f) 20 MHz + 30 MHz, and (g) 10 MHz + 20 MHz + 30 MHz.

TABLE 4. Summary of previous researches for multi-element IVUS transducers.

	Center Frequency	Element Configuration	Electrode Connection Method for Each Element		Housing
			Signal	Ground	
S. Yoon et al. [23]	48/152	Side-to-side	Separately connected to its own central wires of each coaxial cable	Common ground by Cr/Au deposition	Side-looking steel needle
T. Ma et al. [24]	35/90 35/120 35/150	Back-to-back (180°)	Separately connected to its own central and shielding wires of each coaxial cable.		Two-window stainless steel cap
W. Qiu et al. [25]	36/78	Side-to-side	Separately connected to its own coaxial wires for each element	N/A	Side-looking metal housing
J. Lee et al. [26]	35/105	Side-to-side	Separately connected to its own coaxial wires for each element	Common ground by Cr/Au deposition	Side-looking brass tube
J. Lee et al. [27]	35/70	Side-to-side	Separately connected to its own coaxial wires for each element	Common ground by Cr/Au deposition	Side-looking brass tube
C. E. Munding et al. [28],[29]	30/80	Back-to-back (180°)	Separately connected to its own central and shielding wires of each coaxial cable.		Fixed to the end of a torque cable
M. Su et al. [34]	33.8/80	Back-to-back (180°)	Commonly connected to one coaxial cable.	Common ground by Cr/Au deposition	Side-looking two-window copper housing
Z. Li et al. [35]	13/20/30	Back-to-back (120°)	Separately connected to its own central and shielding wires of each coaxial cable.		Need additional support frame to support the elements and isolation filler between elements

is shown in the cyst area and the other one in the background area. Note that the boxes had the same depth and size each other for more accurate comparison. Consequently, the CNR values were calculated using the following equation:

$$\mathrm{CNR} = \frac{|\mu_c - \mu_b|}{\sqrt{\sigma_c^2 + \sigma_b^2}}$$

where μ_c and μ_b are the mean value of signal magnitudes in the cyst and background boxes. σ_c and σ_b are the standard deviations of each region, respectively. As a result, the fundamental images had the CNR values of 3.36, 3.61, and 3.65 for 10 MHz, 20 MHz, and 30 MHz, respectively. On the other hand, the frequency compound images obtained the CNR values of 5.10, 5.11, and 5.12 from the combination

of 10 MHz and 20 MHz, 10 MHz and 30 MHz, and 20 MHz and 30 MHz, respectively. Lastly, the frequency compound image composed of three fundamental images from 10 MHz, 20 MHz, and 30 MHz components had the CNR value of 6.27. It can be seen that the CNR value of the frequency compound image is proportional to the mixed frequency values and the number of frequencies. The measured CNR values were summarized Table 3.

IV. DISCUSSION

In this study, we designed and fabricated a triple-element back-to-back IVUS transducer with a 3D printed housing. It has been well known that the back-to-back configuration for dual-element transducer can achieve a small outer diameter and short length of front-rigid region. In the proposed triple-element structure, the usable operating frequency can be extended while maintaining the advantages of the conventional back-to-back structure by adding a stack composed of a piezoelectric layer and a matching layer on the side of the back-to-back configuration. Also, three elements have a common backing layer and can be successfully integrated using split-assembling technique without additional support frame and isolation filler which were required in the previously conducted study [35]. Furthermore, the proposed triple-element transducer allows to perform image alignment or co-registration by simply rotating the other two images around the center image by $-90°$ and $90°$, respectively.

In order to compare the performance of the proposed technique with other methods, the studies related to the configuration of the multi-frequency transducer for general intravascular imaging and the electrode connection method are summarized in Table 4. Although comparison of image quality between our research and other previous studies was not able to perform due to different experimental setup including target and equipments, regarding to this study, we conducted the evaluation of each image we obtained with respect to axial and lateral beam widths, penetration depth, and CNR. The spatial resolution was enhanced as the center frequency increased, while the penetration depth was improved as the center frequency decreased. On the other hand, CNR values were almost same in all fundamental images since CNR is not affected by center frequency. However, it was proved that CNR was improved by conducting frequency compounding, especially by combining all of three fundamental images obtained by the proposed triple-element transducer.

In the IVUS transducer fabrication process, an electrode connection method can be largely divided into two types as described in Table 4; gold sputtering or wire connection. The former method relatively complicates the manufacturing process and increases the production cost since it involves additional sputtering procedure. Thus, in general, the electrode is formed by connecting the shielding wire of a micro-coaxial wire to the backing layer of an acoustic stack while connecting the central wire to the matching layer of the acoustic stack. However, it is very challenging to place the wire on a surface of very small IVUS element and to fix them with conductive adhesive. In addition, the area blocked by the wire and adhesive should be minimized to maintain proper sensitivity without disturbing the propagation of ultrasound beam. In this regard, the proposed IVUS housing can be an efficient method to reduce the complexity of electrode formation by placing only a small amount of adhesive on the stack. In addition, the proposed IVUS housing enables the simultaneous connection of one signal wire to three elements, which is relatively difficult to realize with the conventional electrode connection method. In this study, although the electrode pattern was formed by filling the engraved grooves with conductive epoxy, if the IVUS housing with already formed the electrode pattern is manufactured, the electrode connection can be conducted more simply by just placing the acoustic stack on the housing and applying the adhesive.

As a result of the property measurement, the electrical impedance decreased as the frequency increases since the element size was fixed and could not be changed due to the size of IVUS housing. Nevertheless, the acoustic stacks were designed to have similar sensitivities using different piezoelectric materials each other when the driving functions with the same voltage were applied to three elements. In the case of pulse-echo test result, although the center frequencies were slightly different from the desired values, due to the fabrication errors occurred in the lapping process, they can still be used in this study since the frequency bands were not overlapped each other and expected to be sufficient to verify the performance of the proposed transducer.

In the process of image acquisition, the proposed transducer uses a single coaxial cable to drive three elements simultaneously, resulting in energy loss compared to individual connection. However, as a result of B-mode imaging, it was found that the energy of each element was still sufficient to acquire an ultrasound image. In addition, the band pass filter successfully removed unwanted frequency components due to simultaneous driving and extracted the desired signal. Also, the imaging system can be simplified by using a single coaxial cable.

In the wire phantom B-mode imaging test, it was confirmed that the axial and lateral resolution were improved as the center frequency increased, as is well known. In the case of the tissue-mimicking phantom B-mode images, the fundamental image with the lowest frequency (Fig. 10(a)) had the deepest penetration depth and poor spatial resolution, while the fundamental image with the highest frequency (Fig. 10(c)) had the most improved spatial resolution and the shallow penetration depth. The fundamental image with the middle frequency (Fig. 10(b)) had an intermediate depth of penetration and spatial resolution. Subsequently, when two of the three fundamental images were combined for the frequency compounding, the CNR values of Fig. 10(d)-(f) increased by 46.34%, 45.79%, and 41.05%, respectively, above the average CNR value of the used fundamental images. Furthermore, the frequency compound image composed of all three fundamental images (Fig. 10(g)) had about 77.12% increased CNR

value. Consequently, the proposed triple-element transducer can achieve various combinations and improved quality of images.

There were some issues about this research. First, the size of the acoustic stack was 1.8 mm × 1.8 mm, which is relatively large for intravascular application. That is due to the technical limitation on the manufacturing current 3D printed housing such as minimum wall thickness and restricted hole diameter. If a smaller IVUS housing can be fabricated with advances in 3D printing technique, it is expected that the acoustic stack of a size more suitable for intravascular imaging will be possible. Second, in this study, two types of piezoelectric elements were used because it is very difficult to change the size of the element due to the aforementioned limitation, and at the same time, it is necessary to maximize the sensitivity by minimizing the electrical impedance mismatch. For the same reason, in this study, the highest frequency was determined as 30 MHz, but in order to maximize the advantages of the proposed triple-element structure, it is necessary to develop a higher frequency element. Thus, it is expected that more optimized design and manufacturing technique will be required. Third, the fabrication of triple-element acoustic stack is relatively complicated than dual-element acoustic stack. However, compared to the previously studied triple-element transducer for endoscopic imaging [31], the proposed transducer still has structural and manufacturing advantages. It does not require additional support frame or isolation filler for coupling three elements since the proposed acoustic stack consists of combined backing layers capable of supporting each element. Thus, it is expected that manufacturing process can be simplified, and the cost can be reduced than the existing one. Despite these issues, in this study, a three-element transducer was successfully developed using a special manufacturing process and a 3D printed housing as a feasibility study.

V. CONCLUSION

In this study, a novel IVUS transducer with triple-element back-to-back structure of acoustic stack was proposed. The fabrication process of the proposed technique and system complexity can be simplified by using split-assembling fabrication scheme, a specially designed 3D printed housing with patterning electrodes, and a single micro-coaxial cable. The proposed transducer can select various frequency options according to the desired imaging area and achieve more improved CNR and higher image accuracy through the frequency compounding technique. Thus, the proposed TEBB_IVUS transducer is expected to be one of the useful methods for diagnosing vascular diseases.

REFERENCES

[1] T. Ma, B. Zhou, T. K. Hsiai, and K. K. Shung, "A review of intravascular ultrasound-based multimodal intravascular imaging: The synergistic approach to characterizing vulnerable plaques," *Ultrason. Imag.*, vol. 38, no. 5, pp. 314–331, Sep. 2016.

[2] F. D. Kolodgie, A. P. Burke, A. Farb, H. K. Gold, J. Yuan, J. Narula, A. V. Finn, and R. Virmani, "The thin-cap fibroatheroma: A type of vulnerable plaque: The major precursor lesion to acute coronary syndromes," *Current Opinion Cardiol.*, vol. 16, no. 5, pp. 285–292, Sep. 2001.

[3] J. Li, X. Li, J. Jing, D. Mohar, A. Raney, S. Mahon, M. Brenner, Q. Zhou, P. Patel, K. K. Shung, and Z. Chen, "Integrated intravascular optical coherence tomography (OCT)—Ultrasound (US) catheter for characterization of atherosclerotic plaques *in vivo*," in *Proc. Annu. Int. Conf. IEEE Eng. Med. Biol. Soc.*, Aug./Sep. 2012, pp. 3175–3178.

[4] A. P. Burke, A. Farb, G. T. Malcom, Y.-H. Liang, J. Smialek, and R. Virmani, "Coronary risk factors and plaque morphology in men with coronary disease who died suddenly," *New England J. Med.*, vol. 336, no. 18, pp. 1276–1282, May 1997.

[5] S. E. Nissen and P. Yock, "Intravascular ultrasound: Novel pathophysiological insights and current clinical applications," *Circulation*, vol. 103, no. 4, pp. 604–616, Jan. 2001.

[6] G. J. Ughi, T. Adriaenssens, P. Sinnaeve, W. Desmet, and J. D'hooge, "Automated tissue characterization of *in vivo* atherosclerotic plaques by intravascular optical coherence tomography images," *Biomed. Opt. Exp.*, vol. 4, no. 7, pp. 1014–1030, Jul. 2013.

[7] H. Jia *et al.*, "*In vivo* diagnosis of plaque erosion and calcified nodule in patients with acute coronary syndrome by intravascular optical coherence tomography," *J. Amer. College Cardiol.*, vol. 62, no. 19, pp. 1748–1758, Nov. 2013.

[8] H. M. Garcia-Garcia, M. A. Costa, and P. W. Serruys, "Imaging of coronary atherosclerosis: Intravascular ultrasound," *Eur. Heart J.*, vol. 31, pp. 2456–2469, Oct. 2010.

[9] I.-K. Jang, B. E. Bouma, D.-H. Kang, S.-J. Park, S.-W. Park, K.-B. Seung, K.-B. Choi, M. Shishkov, K. Schlendorf, E. Pomerantsev, S. L. Houser, H. T. Aretz, and G. J. Tearney, "Visualization of coronary atherosclerotic plaques in patients using optical coherence tomography: Comparison with intravascular ultrasound," *J. Amer. College Cardiol.*, vol. 39, no. 4, pp. 604–609, Feb. 2002.

[10] M. C. McDaniel, P. Eshtehardi, F. J. Sawaya, J. S. Douglas, and H. Samady, "Contemporary clinical applications of coronary intravascular ultrasound," *JACC Cardiovascular Intervent.*, vol. 4, no. 11, pp. 1155–1167, Nov. 2011.

[11] A. V. Finn, M. Nakano, J. Narula, F. D. Kolodgie, and R. Virmani, "Concept of vulnerable/unstable plaque," *Arteriosclerosis, Thrombosis, Vascular Biol.*, vol. 30, no. 7, pp. 1282–1292, Jul. 2010.

[12] N. Shammas, Q. Radaideh, W. J. Shammas, G. E. Daher, R. J. Rachwan, and Y. Radaideh, "The role of precise imaging with intravascular ultrasound in coronary and peripheral interventions," *Vascular Health Risk Manage.*, vol. 15, pp. 283–290, Aug. 2019.

[13] K. Jansen, G. van Soest, and A. F. W. van der Steen, "Intravascular photoacoustic imaging: A new tool for vulnerable plaque identification," *Ultrasound Med. Biol.*, vol. 40, no. 6, pp. 1037–1048, Jun. 2014.

[14] S. Yoon, J. Williams, B. J. Kang, C. Yoon, N. Cabrera-Munoz, J. S. Jeong, S. G. Lee, K. K. Shung, and H. H. Kim, "Angled-focused 45 MHz PMN-PT single element transducer for intravascular ultrasound imaging," *Sens. Actuators A, Phys.*, vol. 228, pp. 16–22, Jun. 2015.

[15] M. E. Brezinski, G. J. Tearney, N. J. Weissman, S. A. Boppart, B. E. Bouma, M. R. Hee, A. E. Weyman, E. A. Swanson, J. F. Southern, and J. G. Fujimoto, "Assessing atherosclerotic plaque morphology: Comparison of optical coherence tomography and high frequency intravascular ultrasound," *Heart*, vol. 77, no. 5, pp. 397–403, May 1997.

[16] M. R. Elliott and A. J. Thrush, "Measurement of resolution in intravascular ultrasound images," *Physiolog. Meas.*, vol. 17, no. 4, pp. 259–265, Nov. 1996.

[17] C. V. Bourantas, F. A. Jaffer, F. J. Gijsen, G. van Soest, S. P. Madden, B. K. Courtney, A. M. Fard, E. Tenekecioglu, Y. Zeng, A. F. W. van der Steen, S. Emelianov, J. Muller, P. H. Stone, L. Marcu, G. J. Tearney, and P. W. Serruys, "Hybrid intravascular imaging: Recent advances, technical considerations, and current applications in the study of plaque pathophysiology," *Eur. Heart J.*, vol. 38, no. 6, pp. 400–412, Feb. 2017.

[18] M. A. Syed and J. M. Hodgson, "Enhanced IVUS: Advances allowing higher resolution and integrated devices," *Current Cardiovascular Imag. Rep.*, vol. 9, no. 8, pp. 1–9, Aug. 2016.

[19] J. Lee, J. Jang, and J. H. Chang, "Oblong-shaped-focused transducers for intravascular ultrasound imaging," *IEEE Trans. Biomed. Eng.*, vol. 64, no. 3, pp. 671–680, Mar. 2017.

[20] J. Yuan, S. Rhee, and X. N. Jiang, "60 MHz PMN-PT based 1–3 composite transducer for IVUS imaging," in *Proc. IEEE Ultrason. Symp.*, Nov. 2008, pp. 682–685.
[21] J. Sung and J. Jeong, "Development of high-frequency (>60 MHz) intravascular ultrasound (IVUS) transducer by using asymmetric electrodes for improved beam profile," *Sensors*, vol. 18, no. 12, p. 4414, Dec. 2018.
[22] X. Li, Q. Zhou, K. K. Shung, W.-H. Shih, and W. Y. Shih, "Novel PMN-PT free standing film for high frequency (80 MHz) intravascular ultrasonic imaging," *IEEE Trans. Ultrason., Ferroelectr., Freq. Control*, vol. 58, no. 11, pp. 2281–2288, Nov. 2011.
[23] S. Yoon, M. G. Kim, J. A. Williams, C. Yoon, B. J. Kang, N. Cabrera-Munoz, K. K. Shung, and H. H. Kim, "Dual-element needle transducer for intravascular ultrasound imaging," *J. Med. Imag.*, vol. 2, no. 2, Apr. 2015, Art. no. 027001.
[24] T. Ma, M. Yu, Z. Chen, C. Fei, K. K. Shung, and Q. Zhou, "Multi-frequency intravascular ultrasound (IVUS) imaging," *IEEE Trans. Ultrason., Ferroelectr., Freq. Control*, vol. 62, no. 1, pp. 97–107, Jan. 2015.
[25] W. Qiu, Y. Chen, C. M. Wong, B. Liu, J. Dai, and H. Zheng, "A novel dual-frequency imaging method for intravascular ultrasound applications," *Ultrasonics*, vol. 57, pp. 31–35, Mar. 2015.
[26] J. Lee, J.-Y. Moon, and J. Chang, "A 35 MHz/105 MHz dual-element focused transducer for intravascular ultrasound tissue imaging using the third harmonic," *Sensors*, vol. 18, no. 7, p. 2290, Jul. 2018.
[27] J. Lee and J. H. Chang, "Dual-element intravascular ultrasound transducer for tissue harmonic imaging and frequency compounding: Development and imaging performance assessment," *IEEE Trans. Biomed. Eng.*, vol. 66, no. 11, pp. 3146–3155, Nov. 2019.
[28] C. E. Munding, E. Chérin, I. Jourard, J. J. Weyers, D. E. Goertz, B. K. Courtney, and F. S. Foster, "Development of a 3 French dual-frequency intravascular ultrasound catheter," *Ultrasound Med. Biol.*, vol. 44, no. 1, pp. 251–266, Jan. 2018.
[29] C. E. Munding, E. Chérin, N. Alves, D. E. Goertz, B. K. Courtney, and F. S. Foster, "30/80 MHz bidirectional dual-frequency IVUS feasibility evaluated *in vivo* and for stent imaging," *Ultrasound Med. Biol.*, vol. 46, no. 8, pp. 2104–2112, Aug. 2020.
[30] J. Ma, K. H. Martin, P. A. Dayton, and X. Jiang, "A preliminary engineering design of intravascular dual-frequency transducers for contrast-enhanced acoustic angiography and molecular imaging," *IEEE Trans. Ultrason., Ferroelectr., Freq. Control*, vol. 61, no. 5, pp. 870–880, May 2014.
[31] J. Ma, X. Jiang, K. H. Martin, P. A. Dayton, Y. Li, and Q. Zhou, "Dual frequency transducers for intravascular ultrasound super-harmonic imaging and acoustic angiography," in *Proc. IEEE Int. Ultrason. Symp.*, Sep. 2014, pp. 675–678.
[32] C. Peng, H. Wu, S. Kim, X. Dai, and X. Jiang, "Recent advances in transducers for intravascular ultrasound (IVUS) imaging," *Sensors*, vol. 21, no. 10, p. 3540, May 2021.
[33] C. C. Shih, P.-Y. Chen, T. Ma, Q. Zhou, K. K. Shung, and C.-C. Huang, "Development of an intravascular ultrasound elastography based on a dual-element transducer," *Roy. Soc. Open Sci.*, vol. 5, no. 4, Apr. 2018, Art. no. 180138.
[34] M. Su, Z. Zhang, J. Hong, Y. Huang, P. Mu, Y. Yu, R. Liu, S. Liang, H. Zheng, and W. Qiu, "Cable-shared dual-frequency catheter for intravascular ultrasound," *IEEE Trans. Ultrason., Ferroelectr., Freq. Control*, vol. 66, no. 5, pp. 849–856, May 2019.
[35] Z. Li, J. Xu, X. Zhu, Z. Han, J. Lv, X. Jian, W. Shao, Y. Jiao, and Y. Cui, "A triple-frequency transducer for endoscopic imaging: Simulation design and experimental verification," *Sens. Actuators A, Phys.*, vol. 321, Apr. 2021, Art. no. 112589.

HEE SU LEE (Student Member, IEEE) received the B.S. degree in biomedical engineering from Dongguk University, Seoul, South Korea, in 2020, where she is currently pursuing the M.S. degree. Her current research interests include intravascular ultrasound transducer and acoustic radiation force impulse imaging.

JONG SEOB JEONG (Member, IEEE) received the B.S. and M.S. degrees in electronic engineering from Sogang University, Seoul, South Korea, in 1999 and 2001, respectively, and the Ph.D. degree in biomedical engineering from the University of Southern California, Los Angeles, CA, USA, in 2010. From 2001 to 2005, he worked at Samsung Electronics Company Ltd., Suwon, South Korea. From 2010 to 2011, he was a Postdoctoral Research with the NIH Resource Center for Medical Ultrasonic Transducer Technology, Department of Biomedical Engineering, University of Southern California, Los Angeles. He is currently an Associate Professor with the Department of Biomedical Engineering, Dongguk University, Seoul. His research interests include medical signal processing and systems and the development of ultrasound transducers for diagnosis and therapy.